



Open Archive Toulouse Archive Ouverte


OATAO is an open access repository that collects the work of Toulouse researchers and makes it freely available over the web where possible

This is an author's version published in:

<http://oatao.univ-toulouse.fr/26626>

Official URL

DOI : <https://doi.org/10.1016/J.MATCHAR.2019.05.020>

To cite this version: Bellavoine, Marion and Dumont, Myriam and Dehmas, Moukrane  and Stark, Andreas and Schell, Norbert and Drillet, Josée and Hébert, Véronique and Maugis, Philippe *Ferrite recrystallization and austenite formation during annealing of cold-rolled advanced high-strength steels: In situ synchrotron X-ray diffraction and modeling.* (2019) *Materials Characterization*, 154. 20-30. ISSN 1044-5803

Any correspondence concerning this service should be sent to the repository administrator: tech-oatao@listes-diff.inp-toulouse.fr

Ferrite recrystallization and austenite formation during annealing of cold-rolled advanced high-strength steels: In situ synchrotron X-ray diffraction and modeling

Marion Bellavoine^{a,b}, Myriam Dumont^{a,*}, Moukrane Dehmas^c, Andreas Stark^d, Norbert Schell^d, Josée Drillet^b, Véronique Hébert^b, Philippe Maugis^a

^a Aix Marseille Univ, Univ. Toulon, CNRS, IM2NP, Marseille, France

^b ArcelorMittal Research SA, Maizières-les-Metz, France

^c CIRIMAT, Université de Toulouse, CNRS, Toulouse, France

^d Institute of Materials Research, Helmholtz-Zentrum Geesthacht Centre for Materials and Coastal Research, Geesthacht, Germany

ARTICLE INFO

Keywords:

Dual phase steels

Recrystallization

Austenite formation

Annealing

ABSTRACT

Ferrite recrystallization and austenite formation occurring during annealing of cold-rolled advanced high-strength steels are key mechanisms as they largely determine the final microstructure and mechanical properties. However, the influence of processing parameters on these mechanisms and their interactions is still not fully understood. This is particularly the case for Dual-Phase steels having an initial cold-rolled microstructure consisting of ferrite and martensite before annealing, which were scarcely investigated compared to ferrite-pearlite initial microstructures. In situ synchrotron X-ray diffraction experiments together with post-mortem metallographic analysis allowed clarifying both ferrite recrystallization and austenite formation during annealing of a ferrite-martensite initial microstructure depending on the process parameters of the annealing cycle. Results showed a major influence of recrystallization state on austenite formation, leading to an unexpected effect of heating rate on austenite formation kinetics. A modeling approach was undertaken to rationalize the influence of heating rate on austenite formation by taking into account the bi-phased ferrite-martensite initial microstructure and the effect of ferrite recrystallization state.

1. Introduction

The steel industry is facing great challenges in the development of advanced high-strength steels designed to improve the fuel efficiency of automobiles without compromising their safety, performance and affordability. Dual Phase (DP) steels have been developed for this purpose and have become reference materials for these applications. They offer significant weight-saving potential thanks to their high strength and exhibit a good compromise between strength and formability [1–3]. The final microstructure of DP steels consists of hard martensite islands dispersed in ferritic and sometimes bainitic matrix. Processing steps for cold-rolled products include successive hot-rolling, cold-rolling, annealing and subsequent cooling. Annealing of cold-rolled sheets consists in heating and soaking in the intercritical temperature range, producing a mixture of ferrite and austenite phases. Austenite decomposition during cooling leads to the final Dual Phase microstructure. As the final

microstructure directly inherits from the austenite-ferrite mixture obtained at the end of annealing, a broad knowledge of microstructure formation during this stage is of prime importance for the design of industrial processing routes. Microstructure formation during annealing is the result of two major mechanisms: ferrite recrystallization and austenite formation. They can occur simultaneously or successively and can interact with each other depending on their kinetics. The influence of processing parameters of the annealing cycle (heating rate, soaking temperature and soaking time) on the kinetics and interactions of these mechanisms has thus received much attention. The experimental studies dealing with annealing of cold-rolled DP steel grades agree that rapid heating leads to delayed recrystallization [4–7]. Understanding austenite formation kinetics depending on process parameters is much more complex. Huang et al. [5] found that austenite formation during heating of a Fe–C–Mn–Si steel with a ferrite-pearlite initial cold-rolled microstructure is delayed when increasing the heating rate from 1 °C/s

* Corresponding author at: IM2NP – UMR CNRS 7334 – Aix-Marseille Université, Faculté des Sciences et Techniques de St-Jérôme, Service 251, 13 397 Marseille Cedex 20, France.

E-mail address: myriam.dumont@univ-amu.fr (M. Dumont).

to 100 °C/s. A similar behavior was also observed by Azizi-Alizami et al. [8] in a cold-rolled low carbon steel with a ferrite-pearlite initial microstructure. On the contrary, in a cold-rolled Fe-C-Mn-Mo steel presenting also a ferrite-pearlite initial microstructure, the austenite fraction as a function of temperature was found to be independent of heating rate in the range 1 to 100 °C/s by Huang et al. [5], i.e. the rate of austenite formation increases with heating rate accordingly and was then e.g. 100 times faster at 100 °C/s as compared to 1 °C/s. This was also observed by other authors in Fe-C-Mn-Si cold-rolled DP steels [9,10]. Besides, Chbihi et al. [7] observed that the volume fraction of austenite is much higher after continuous heating at 100 °C/s than at 1 °C/s. Kulakov et al. [11] also observed the formation of a higher austenite fraction in case of rapid heating for a Fe-C-Mn-Si-Cr grade having a ferrite-pearlite-bainite initial microstructure. Studies dealing with a ferrite-martensite initial microstructure are very few: Philippot et al. [6] showed that increasing the heating rate from 1 °C/s to 10 °C/s has very little effect on austenite volume fraction formed during heating. However, all studies [5-7,9,11] agree that increasing the heating rate favors the overlap of ferrite recrystallization and austenite formation, which results in a finer and more heterogeneous microstructure inheriting from the initial cold-rolled microstructure. They also revealed a significant acceleration of austenite growth during isothermal soaking when increasing the heating rate. This behavior is mainly attributed to the delayed recrystallization of ferrite, which is thought to provide additional nucleation sites for austenite and enhance the growth rate of austenite thanks to high density of defects in non-recrystallized ferrite [11].

The difficulty in understanding and predicting austenite formation kinetics depending on process parameters thus relies on this effect of recrystallization state. As recrystallization state also depends on other factors including the microstructure obtained after cold-rolling [11] and the nominal composition [12,13] which in turn affect austenite formation, the kinetics and interactions of ferrite recrystallization and austenite formation can be very different for various steels.

In order to bring some clarifications regarding this microstructure development coming from the interrelation of ferrite recrystallization and austenite formation in the case of a ferrite-martensite initial cold-rolled microstructure, the present study investigates both mechanisms during annealing of a cold-rolled Dual Phase steel grade using various heating rates and complementary experimental techniques of in situ synchrotron X-ray diffraction and post-mortem metallographic analysis.

2. Materials and experimental procedure

The steel under investigation is a low carbon Dual Phase steel. Its nominal composition is 0.075C-2.5Mn-0.3Cr-0.3Si-0.028Nb-0.027Ti-0.002B-0.004N-Fe (balance) (in weight percent). Laboratory ingots were obtained from a slab pilot caster and hot-rolled followed by cold-rolling down to a thickness of 1.25 mm. The microstructure obtained after cold-rolling and before annealing is composed of martensite islands (30% ± 5%) embedded in a ferrite matrix (Fig. 1).

Recrystallization kinetics during annealing was investigated by post-mortem metallographic analysis and austenite formation kinetics was determined by metallographic analysis and in situ synchrotron X-ray diffraction.

Post-mortem metallographic analysis was carried out after continuous heating of cold-rolled sheets (12 mm length and section of 3 × 1.25 mm²) using DT 1000 thermal simulator and interrupted at different temperatures between 650 °C and 830 °C by helium blowing. Heating rates of either 1 °C/s or 10 °C/s were used. Cooling rates were higher than 300 °C/s to transform the austenite into fresh martensite during cooling. The annealed samples were prepared by standard metallographic techniques, etched with Dino solution (140 ml of distilled water, 100 ml of H₂O₂, 4 g of oxalic acid, 2 ml of H₂SO₄, and 1.5 ml of HF) and observed at ¼ of the sheet thickness using FEG-SEM JEOL® JSM-7800F microscope. Non-recrystallized ferrite zones are elongated

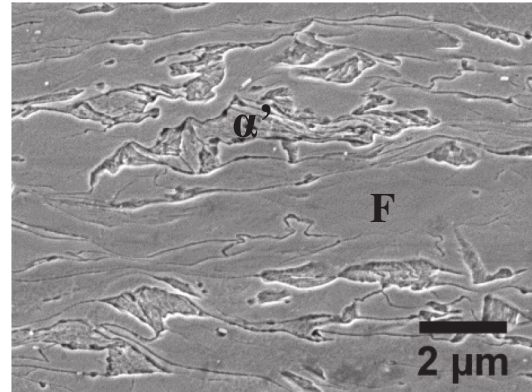


Fig. 1. Initial microstructure of the cold-rolled sheet made of martensite (α') and ferrite (F) (SEM micrograph).

and appear with surface irregularities whereas recrystallized ferrite grains are polygonal and appear with a smooth surface. Fresh martensite is strongly etched and has a typical rough aspect. Phase fractions were obtained by manual phase identification and image analysis of FEG-SEM images.

In situ synchrotron high-energy X-ray diffraction (HEXRD) analysis was carried out at beamline P07B of PETRA III storage ring in DESY (Deutsches Elektronen-Synchrotron, Hamburg, Germany). The experimental set-up was composed of a Bähr DIL805 A/D dilatometer modified with two windows on the beam path and a 2-D image plate detector. The measurements were conducted in transmission geometry using a photon energy of 87 keV (wavelength $\lambda = 0.1425$ Å) and a beam size of 0.7 × 0.7 mm². Samples of 7 mm length and section of 4 × 1.25 mm² were cut from the cold-rolled sheets and mounted on the dilatometer so that the incoming X-ray beam made a 45° angle with the sample length direction to limit the effect of texture coming from the successive hot-rolling and cold-rolling steps. The sample was heated up by an induction coil open in the middle so that the beam passes only through the sample [14]. Temperature measurements were recorded by Pt/Pt-Rh thermocouples which were spot-welded on the 7 mm × 4 mm surface of the sample. The dilatometer chamber was maintained under vacuum (5·10⁻² Pa) during the experiment. Heat treatment cycles consisted in continuous heating using five different heating rates (0.25, 1, 5, 10 and 50 °C/s) up to 900 °C followed by He blowing. Cycles composed of continuous heating at 1 or 10 °C/s followed by 120 s soaking at 700 °C, 750 °C and 790 °C were also carried out. The diffraction patterns were recorded by a 2-D image plate detector Perkin Elmer XRD 1621 with a pixel size of 200 μm and a pixel grid of 2048 × 2048 with an acquisition time of 0.1 s. The small wavelength led to small diffraction angles (< 10°) and allowed the collection of complete sets of Debye-Scherrer rings. Fit2D software [15] was used for the integration of the diffracted intensities according to the azimuthal angles. The geometry of the detector was calibrated with reference to the diffraction geometry using LaB₆ standard powder. Fig. 2 shows an example of raw data consisting of a diffraction pattern recorded during the in situ experiment (Fig. 2(a)) and the corresponding azimuthally integrated diffraction pattern obtained after integration by Fit2D (Fig. 2(b)).

Phase fractions of ferrite and austenite were derived from azimuthally integrated XRD patterns using Rietveld refinement method implemented in FullProf software [16]. The contribution of cementite to the global volume fraction was assumed to be negligible as it could not be detected in the integrated XRD pattern due to insufficient volume fraction and/or size (the estimated maximum volume fraction and size of cementite particles are 1.1%vol. and 150 nm, respectively). A pseudo-Voigt function was selected to describe ferrite and austenite peak shape and for each pattern the cyclic refinement option available in Fullprof was used to refine the following parameters: the

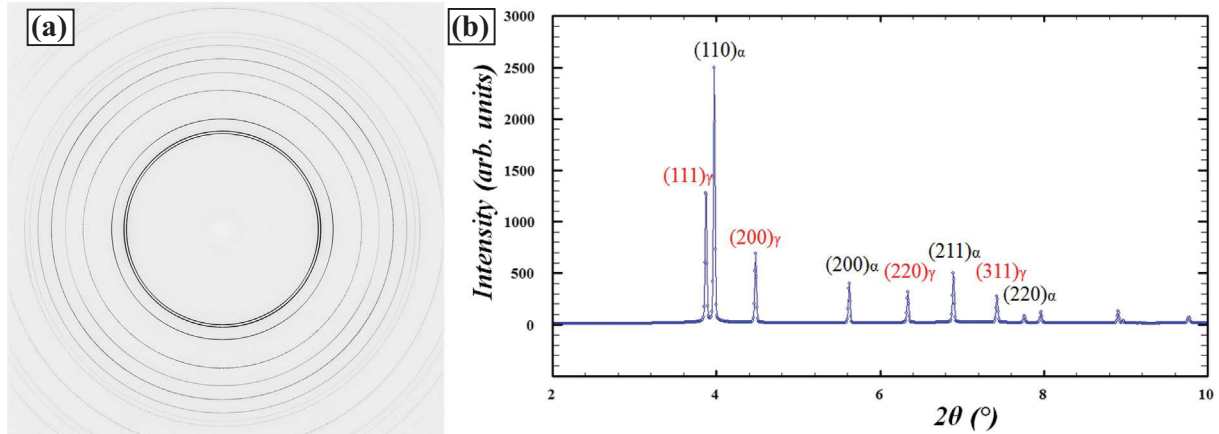


Fig. 2. X-ray diffraction patterns (a) as recorded by the flat panel detector during in situ experiments (b) as obtained after integration with Fit2D software.

background, which was modeled as a polynomial function, scale factors, lattice parameters, peak widths, the peak shape (Gaussian Lorentzian components) and the overall isotropic temperature factor.

Formation of recrystallized ferrite grains is evidenced on XRD patterns by the appearance of sharp spots on Debye-Scherrer rings (Fig. 3(b)). These spots appear and increase in intensity with the formation and growth of recrystallized grains [17]. Visual inspection of XRD patterns thus allows quick estimation of ferrite recrystallization start temperature during heating.

3. Results

3.1. Austenite formation kinetics during continuous heating

3.1.1. In situ synchrotron X-ray diffraction experiments

Austenite formation kinetics during annealing was first investigated using in situ synchrotron X-ray diffraction experiments. The austenite fraction measured by this technique during continuous heating experiments using a broad range of heating rates (0.25, 1, 5, 10, 50 °C/s) is represented in Fig. 4. Comparison of austenite fraction as measured by HEXRD and by image analysis of SEM micrographs (metallography) for 10 °C/s shows a satisfactory agreement.

Results reveal a trend of increasing A_{c1} temperature with increasing heating rate and show that austenite nucleation is shifted towards higher temperatures when increasing the heating rate from 1 °C/s to 10 °C/s. The shift in A_{c1} temperature is however not significant when increasing the heating from 0.25 °C/s to 1 °C/s or from 10 °C/s to 50 °C/s. If A_{c1} temperatures are overall ranging according to the heating rates, the slope of austenite fraction as a function of temperature is slower in

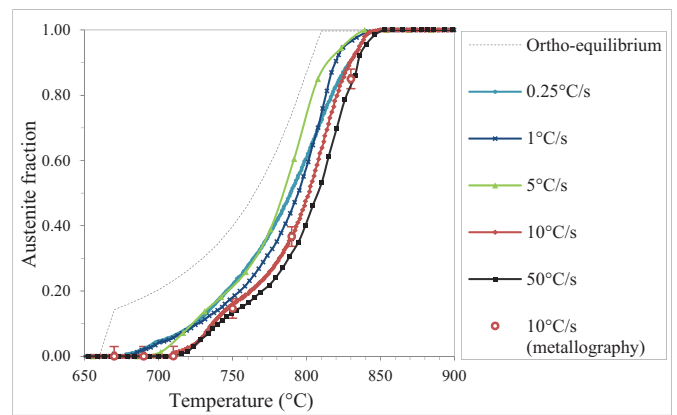


Fig. 4. Austenite fraction formed during continuous heating in case of various heating rates: 0.25, 1, 5, 10 and 50 °C/s (in situ HEXRD results).

case of lower heating rates (0.25 °C/s and 1 °C/s). As a consequence, the austenite fraction formed at a given temperature is not systematically smaller when increasing the heating rate. In particular, austenite fraction formed during heating at 5 °C/s becomes higher than the austenite fraction formed during heating at 1 °C/s for $T > 730$ °C, and it becomes even higher than the austenite fraction formed during heating at 0.25 °C/s for $T > 790$ °C. Thus increasing the heating rate does not systematically result in smaller austenite fraction at a given temperature, as it could be expected for a thermally-activated mechanism.

As ferrite recrystallization state has been reported to have an influence on austenite formation [4–8], ferrite recrystallization was also

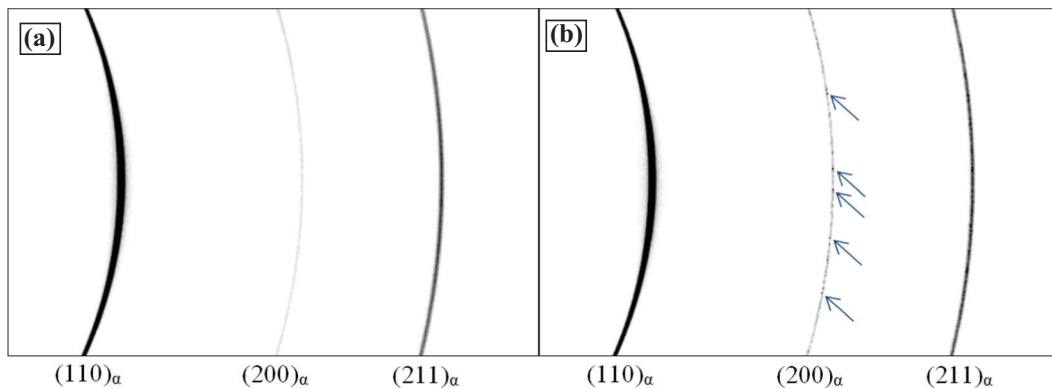


Fig. 3. Evidence of ferrite recrystallization on diffraction patterns during continuous heating at 5 °C/s (a) at 649 °C and (b) at 697 °C. Arrows indicate sharp spots due to recrystallized grains on $\{200\}_\alpha$ ring.

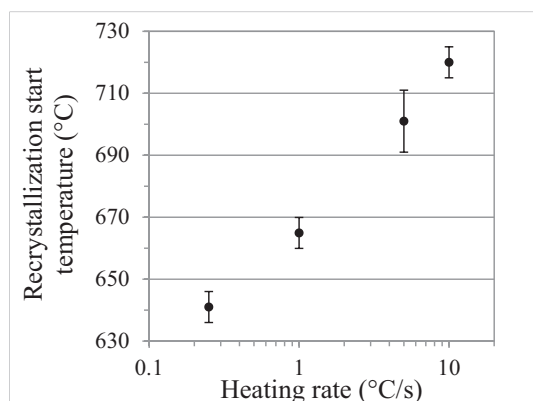


Fig. 5. Ferrite recrystallization starts temperature during continuous heating as a function of heating rate.

investigated by the previously described in situ synchrotron XRD experiments. Recrystallization start temperatures determined by visual inspection of XRD patterns during continuous heating are represented in Fig. 5 for the various investigated heating rates. Results reveal a continuous increase of recrystallization start temperature when increasing heating rate from 0.25 °C/s to 10 °C/s. For the highest heating rate of 50 °C/s, ferrite Debye-Scherrer rings disappear before any appearance of sharp spots, indicating negligible recrystallized ferrite fraction during heating at 50 °C/s. These results clearly show that the recrystallization state when austenite starts to form is significantly different depending on the heating rate.

3.1.2. Post-mortem metallographic analysis

Microstructural changes during continuous heating were further investigated using post-mortem metallographic analysis in the case of two heating rates: 1 °C/s and 10 °C/s. Contrary to XRD results originating from the whole sample thickness, metallographic analyses were conducted in the $\frac{1}{4}$ of the sheet thickness, which classically gives an average representation of the whole microstructure. Examples of microstructural observations are illustrated in Fig. 6.

3.1.2.1. Continuous heating at 1 °/s. Heating the cold-rolled ferrite-martensite microstructure at 1 °C/s until 670 °C leads to a mixture of ferrite and cementite resulting from the tempering of martensite (Fig. 6(a)). Observations reveal the presence of cementite-rich regions corresponding to former martensite islands of the cold-rolled sheet (dotted rectangles in Fig. 6(a)). At 670 °C, ferrite is still mostly non-recrystallized. First recrystallized grains smaller than 1 μ m can however be distinguished in former martensite islands (green arrows in Fig. 6(a)). During heating between 670 °C and 690 °C, ferrite recrystallization progresses by nucleation and growth. At the end of heating at 750 °C, ferrite is almost fully recrystallized (Fig. 6(d)).

First austenite nuclei can be seen at 690 °C (black holes in Fig. 6(b)). These first austenite grains nucleated at triple junctions. Between 690 °C and 710 °C, austenite formation occurs essentially by nucleation (Fig. 6(b) and (c)). Austenite nucleation sites are regions with high cementite density located in former martensite islands, which mostly correspond to triple junctions and recrystallized ferrite grain boundaries. Cementite particles located inside recrystallized ferrite grains are second-order nucleation sites. In case of heating at 1 °C/s, the advanced recrystallization state when austenite nucleates leads to homogeneous spatial distribution of austenite nucleation sites, and thus an homogeneous microstructure composed of austenite grains nucleated around recrystallized ferrite grains (Fig. 6(d)).

3.1.2.2. Comparison of 1°/s and 10°/s heating rates. Comparing the microstructural features obtained in case of slow heating at 1 °C/s and

faster heating at 10 °C/s (Fig. 6(e) and (f)) brings first conclusions about the influence of heating rate on ferrite recrystallization and austenite formation.

Micrographs obtained at the end of heating at 710 °C (Fig. 6(c) and (e)) show that ferrite recrystallization is strongly retarded when increasing the heating rate from 1 °C/s to 10 °C/s: recrystallization has already well progressed when heating at 1 °C/s (Fig. 6(c)) while it has barely started when heating at 10 °C/s. Comparing Fig. 6(c) and (e) also shows that austenite nucleation is delayed when increasing the heating rate. At 710 °C, very few austenite islands are visible after heating at 10 °C/s while a significant amount of austenite islands (blue arrows on (c)) formed during heating at 1 °C/s. Nucleation sites for austenite are identical for the two heating rates: cementite particles located at triple junctions or recrystallized ferrite grain boundaries. However, their spatial distribution and their number are completely different depending on the heating rate. Delayed ferrite recrystallization in case of higher heating rate leads to concentration of austenite nucleation sites in ferrite recrystallized zones coming from former martensite islands. A higher heating rate also results in smaller recrystallized ferrite grain size due to delayed recrystallization but also to smaller and more numerous cementite particles. The number density of austenite nucleation sites is thus higher in case of higher heating rate. The austenite-ferrite microstructure is less homogeneous as it contains some regions composed of a fine mixture of recrystallized ferrite and austenite grains concentrated in the former martensite islands.

The influence of heating rate on ferrite recrystallization state when austenite starts to form thus determines the number and location of austenite nucleation sites. This leads to very different ferrite-austenite microstructures depending on the heating rate.

Phase fractions determined by analysis of SEM images are summarized in Fig. 7. Results confirm that recrystallization kinetics is strongly shifted towards higher temperatures when increasing the heating rate from 1 °C/s to 10 °C/s. However, austenite volume fraction is similar for the two investigated heating rates despite very different microstructures (Fig. 6). Fig. 7 clearly shows that recrystallization has already well progressed when austenite starts to form in case of heating at 1 °C/s while it has barely started in case of heating at 10 °C/s: at the end of heating at 710 °C, non-recrystallized ferrite fraction is 0.16 and 0.96 ($\pm 3\%$ vol.) in case of heating at 1 °C/s and 10 °C/s, respectively.

In order to clarify the influence of heating rate on austenite formation, the density and mean size of austenite grains after continuous heating are represented for the two heating rates of 1 °C/s and 10 °C/s until 790 °C in Fig. 8. Results confirm that austenite nucleation is shifted towards higher temperatures when increasing the heating rate (Fig. 8(b)). They also reveal that higher heating rate leads to higher density of austenite islands but smaller mean area (Fig. 8(a)), resulting in similar austenite fractions compared to the lower heating rate (Fig. 8(c)). Despite the strong effect of heating rate on size and density of austenite islands, austenite fraction as a function of temperature is similar for the two investigated heating rates because the effects of size and density compensate in this case.

3.2. Austenite formation kinetics during isothermal soaking

The evolution of austenite fraction obtained by in situ synchrotron XRD experiments in case of 120 s isothermal soaking after heating at 1 °C/s or 10 °C/s is summarized in Fig. 9. Recrystallized ferrite fractions measured by post-mortem analysis at the beginning of soaking are also presented. They show that recrystallization state is much less advanced after a fast heating at 10 °C/s. XRD results reveal that the increase in austenite fraction during soaking is greater after fast heating. This leads to higher austenite fractions after fast heating from the very beginning of soaking. Austenite fraction at the end of 120 s soaking is higher in case of fast heating and can be higher than the austenite fraction calculated under ortho-equilibrium conditions.

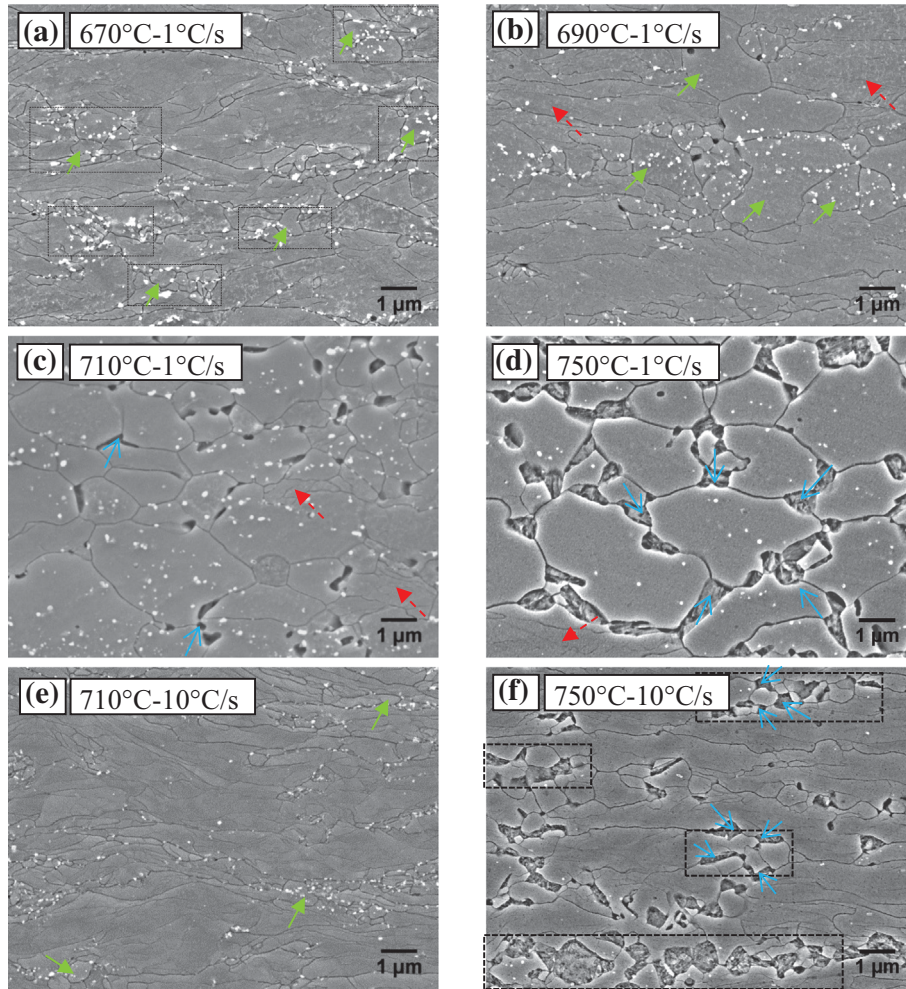


Fig. 6. Microstructures obtained at the end of heating at 1 °C/s at (a) 670 °C (b) 690 °C (c) 710 °C (d) 750 °C and at the end of heating at 10 °C/s at (e) 710 °C and (f) 750 °C (SEM-FEG). Dotted red, full green and open blue arrows indicate non-recrystallized ferrite, first recrystallized grains and austenite islands, respectively. (For interpretation of the references to colour in this figure legend, the reader is referred to the web version of this article.)

4. Discussion

4.1. Effect of heating rate on recrystallization and austenite formation

Both in situ synchrotron XRD experiments and post-mortem metallographic analysis revealed a strong shift of ferrite recrystallization kinetics towards higher temperatures when increasing the heating rate. This shift is due to thermal activation, as reported in the literature [18]:

lower heating rates promote the recrystallization process by increasing the time spent at each temperature.

The effect of heating rate on austenite formation is less obvious. Indeed, experimental results show that austenite formation kinetics is not simply shifted towards higher temperatures with increasing heating rate. In particular, increasing the heating rate can result in higher austenite fraction at a given temperature. These results indicate that the kinetics of austenite formation does not result from a unique thermally-

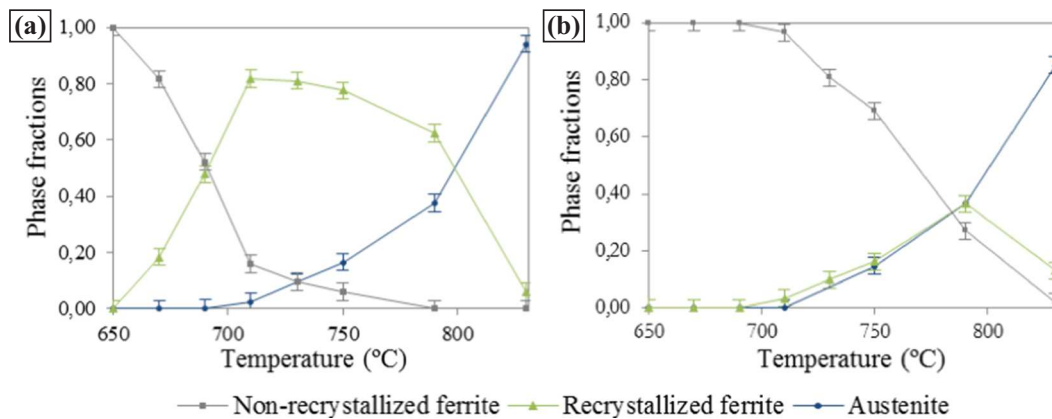


Fig. 7. Phase fractions during continuous heating at (a) 1 °C/s and (b) 10 °C/s.

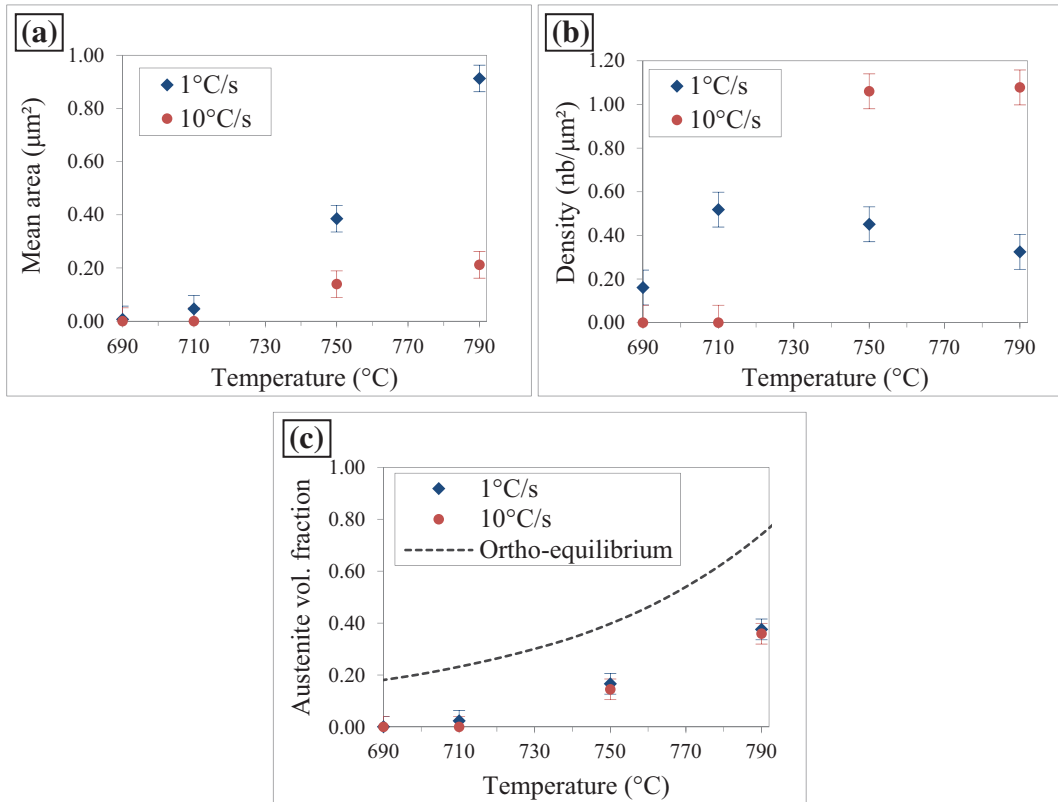


Fig. 8. Evolution of (a) mean area (b) density and (c) volume fraction of austenite islands during continuous heating at 1 °C/s and 10 °C/s.

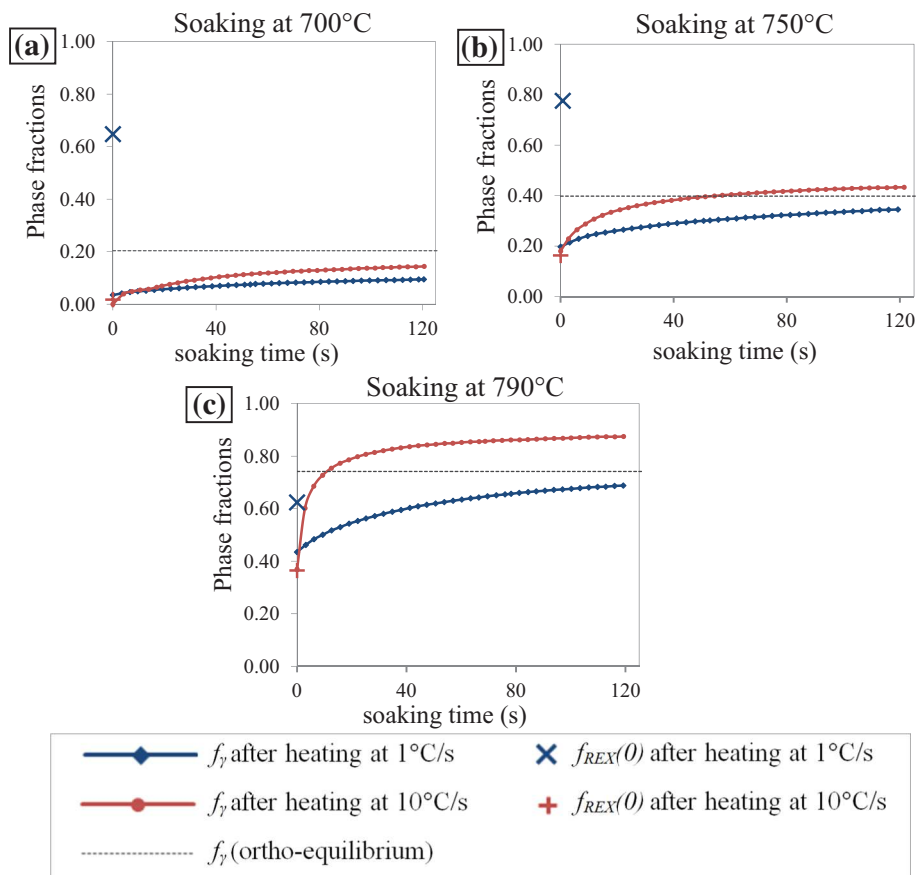


Fig. 9. Austenite fraction measured by in situ XRD during 120 s isothermal soaking and recrystallized ferrite fraction measured by post-mortem analysis at the beginning of soaking at (a) 700 °C (b) 750 °C (c) 790 °C, after heating at 1 °C/s or 10 °C/s.

activated mechanism. They suggest that the promoting effect of higher heating rates on austenite formation is related to the ferrite recrystallization kinetics. Indeed, delayed recrystallization in case of higher heating rate brings several consequences:

- higher density of austenite nucleation sites (Fig. 8(b)),
- faster cementite dissolution kinetics due to its smaller size, which provides C release necessary for the austenite growth [19,20],
- accelerated diffusion in non-recrystallized ferrite due to the presence of defects [21],
- possibly different nature of the local equilibrium at the ferrite-austenite interface [7].

All these consequences are likely to promote austenite formation. Austenite formation kinetics during isothermal soaking also reveals this promoting effect of a high heating rate since austenite fraction is higher from the very beginning of soaking following fast heating. This may be due to the growth of austenite from a superior density of austenite grains at the end of fast heating (Fig. 8(b)). The other factors listed above may also contribute to the accelerated austenite formation during soaking after a fast heating. Our results show that austenite fraction can be higher than the ortho-equilibrium fraction. This has already been observed in other studies [5–7] in case of isothermal soaking treatments applied after fast heating of cold-rolled microstructures. This overrun of maximum fraction may be a transitional regime preceding a decrease of austenite formation after a long time to reach equilibrium.

Another key result is the influence of heating rate on the morphology of the ferrite-austenite microstructure. Increasing the heating rate results in a higher density of austenite nuclei formed in prior martensite regions from the cold-rolled microstructure due to the less advanced recrystallization state. The heating rate has thus a strong impact on the morphology of the microstructure as increasing the heating rate leads to more heterogeneous ferrite-austenite microstructures.

4.2. Modeling ferrite recrystallization and austenite formation during annealing

In order to clarify the influence of heating rate on austenite formation and particularly the influence of ferrite recrystallization on austenite formation, a modeling approach of coupled ferrite recrystallization and austenite formation during annealing is proposed. Some modeling approaches are already present in the literature coupling ferrite recrystallization and austenite formation during intercritical annealing using different degree of complexity from Johnson-Mehl-Avrami-Kolmogorov equations [22,23], phase-field modeling [24] to cellular automaton model [25,26]. The aim of the present modeling approach is to develop a phenomenological approach as simple as possible to rationalize the effects observed experimentally. These effects are (i) the influence of heating rate on austenite formation in the absence of ferrite recrystallization, and (ii) the indirect effect of ferrite recrystallization kinetics on the austenite formation kinetics.

Ferrite recrystallization and austenite formation during annealing of a cold-rolled ferrite-martensite microstructure are modeled using the constitutive equations of Johnson-Mehl-Avrami-Kolmogorov (JMAK) theory [27–29]. The two transformations are treated simultaneously using the approach described by Jones and Bhadeshia [30]. Calculating the variation of recrystallized ferrite fraction $df_{\alpha_{REX}}$ from the variation of extended recrystallized ferrite fraction $df_{\alpha_{REX}}^e$ (Eq. 1) not only involves the recrystallized ferrite fraction but also the austenite fraction:

$$df_{\alpha_{REX}}(t) = (1 - f_{\alpha_{REX}}(t) - f_{\gamma}(t)) \cdot df_{\alpha_{REX}}^e(t). \quad (1)$$

Assuming site saturation, the extended recrystallized fraction is given by (Eq.2):

$$f_{\alpha_{REX}}^e(t) = N_{REX} \cdot \frac{4}{3} \pi \left(\int_0^t M_{REX}(t) E_{REX}(t) dt \right)^3. \quad (2)$$

N_{REX} is the number of recrystallization sites per unit volume, considering that nucleation is instantaneous. The mobility of the recrystallization front M_{REX} is temperature-dependent and the driving force for recrystallization E_{REX} is linked to the stored energy of deformation, determined by the dislocation density ρ :

$$M_{REX}(t) = \frac{D_{gb}^0}{R_{gp} T} \frac{V_{Fe(\alpha)}}{\lambda} \exp\left(-\frac{Q_{gb}}{R_{gp} T}\right), \quad (3)$$

$$E_{REX}(t) = \frac{1}{2} \mu b^2 \rho. \quad (4)$$

D_{gb}^0 and Q_{gb} are respectively the pre-exponential factor and the activation energy for grain boundary mobility, $V_{Fe(\alpha)}$ is ferrite molar volume ($7.11 \text{ cm}^3 \cdot \text{mol}^{-1}$) and λ is the grain boundary thickness (0.25 nm). μ is the shear modulus ($8.10^{10} \text{ J} \cdot \text{m}^{-3}$) and b is the Burgers vector ($2.5 \cdot 10^{-10} \text{ m}$).

The variation in austenite volume fraction is expressed as a function of the variation of the extended austenite fraction (Eq. 5). Austenite is assumed to form both in recrystallized ferrite and non-recrystallized ferrite, and indifferently in these two phases:

$$df_{\gamma}(t) = (1 - f_{\gamma}(t)) \cdot df_{\gamma}^e(t). \quad (5)$$

Considering radial growth geometry for austenite grains, the variation of extended austenite fraction is given by (Eq. 6):

$$\frac{df_{\gamma}^e(t)}{dt} = 4\pi \cdot N_{\gamma} \cdot R_{\gamma}^e(t)^2 \cdot \frac{dR_{\gamma}^e(t)}{dt} \quad (6)$$

where N_{γ} is the number of austenite nucleation sites per unit volume and R_{γ}^e is the extended mean austenite radius. Its growth rate (Eq. 7) can be expressed as a function of the mobility of the α/γ interface $M^{\alpha\gamma}(t)$ and the driving force for $\alpha \rightarrow \gamma$ transformation $\Delta G_{\gamma}(t)$:

$$\frac{dR_{\gamma}^e(t)}{dt} = M^{\alpha\gamma}(t) \cdot \Delta G_{\gamma}(t). \quad (7)$$

Combination of (Eq. 6) and (Eq. 7) gives the growth rate of the extended austenite fraction (Eq. 8):

$$\frac{df_{\gamma}^e(t)}{dt} = (36\pi \cdot N_{\gamma})^{1/3} \cdot f_{\gamma}^e(t)^{2/3} \cdot M^{\alpha\gamma}(t) \cdot \Delta G_{\gamma}. \quad (8)$$

We express the mobility of the α/γ interface by an Arrhenius law:

$$M^{\alpha\gamma}(t) = M_0 \exp\left(-\frac{Q_{\gamma}}{R_{gp} T}\right) \quad (9)$$

with M_0 ($\text{mol} \cdot \text{m} \cdot \text{J}^{-1} \cdot \text{s}^{-1}$) and Q_{γ} ($\text{en J} \cdot \text{mol}^{-1}$) the pre-exponential factor and the activation energy for the interface mobility. ΔG_{γ} is the transformation driving force, expressed as a function of the deviation from the austenite equilibrium fraction f_{γ}^{eq} :

$$\Delta G_{\gamma}(t) = \Delta G_{\gamma 0} (f_{\gamma}^{eq}(t) - f_{\gamma}(t)), \quad (10)$$

where $\Delta G_{\gamma 0}$ ($\text{J} \cdot \text{mol}^{-1}$) is a prefactor for the driving force. The variation of extended austenite volume fraction is finally given by (Eq. 11):

$$\frac{df_{\gamma}^e(t)}{dt} = (36\pi \cdot N_{\gamma})^{1/3} \cdot f_{\gamma}^e(t)^{2/3} \cdot M_0 \cdot \Delta G_{\gamma 0} \exp\left(-\frac{Q_{\gamma}}{R_{gp} T}\right) (f_{\gamma}^{eq}(t) - f_{\gamma}(t)). \quad (11)$$

Experimental results revealed a faster austenite formation in case of less advanced recrystallization state. In particular, the number of austenite nucleation sites is higher (Fig. 8(b)). The influence of recrystallization state on austenite formation can be taken into account in the model by the number of austenite nucleation sites per volume N_{γ} . Expressing N_{γ} as a function of the recrystallized ferrite fraction at

$T = Ae_1$ according to (Eq. 12)

$$N_\gamma = \frac{N_{\gamma 0}}{f_{\alpha REX}(T_{Ae1})} \quad (12)$$

leads to an increasing number of austenite nucleation sites with less advanced recrystallization state.

To model ferrite recrystallization and austenite formation in case of annealing of a bi-phased ferrite-martensite cold-rolled microstructure, the modeled system is divided into two sub-systems representing the two phases of the initial cold-rolled microstructure: ferrite and martensite. The two sub-systems differ in dislocation density, assumed to be higher in martensite. Higher dislocation density leads to higher recrystallization driving force in martensite, which is consistent with the experimental results showing that ferrite recrystallization initiates in former martensite islands of the cold-rolled sheets. The phases also differ by their composition, especially in C and Mn. This is expected to affect the kinetics in the same way as the dislocation density, i.e. higher C and Mn lead to larger rates for austenite formation. Therefore, the parameter ρ in the model accounts for both differences in composition and in dislocation density. The behavior of the full system is obtained by a summation of the two sub-systems weighted by their volume fraction in the cold-rolled sheet (70% ferrite and 30% martensite). The values of adjustable parameters used in the model are summarized in Table 1.

Applying the model using a fixed number of austenite nucleation sites equal to $N_{\gamma 0}$ for the various heating rates allows the prediction of the expected austenite fraction if there were no influence of ferrite recrystallization. Modeling results in this case are represented in Fig. 10 and show that austenite formation is strongly shifted towards higher temperatures, which is expected in case of a thermally activated mechanism. The predicted austenite fraction remains close to zero for the highest heating rate of 50 °C/s while it is closer to equilibrium fraction for the lower heating rate of 0.25 °C/s.

Taking into account the influence of recrystallization state on austenite formation results in the modeled austenite kinetics displayed in Fig. 11(b) in case of continuous heating. Fig. 11(a) represents the modeled recrystallized ferrite fraction and shows that modeling results reproduce the shift of the recrystallization mechanism towards higher temperatures when increasing the heating rate. Introducing the influence of ferrite recrystallization state on austenite formation results in accelerated kinetics of austenite formation in case of increasing heating rates (Fig. 11(b)). The promoting effect of a delayed recrystallization process leads to limited sensitivity of austenite fraction to the heating rate (Fig. 11(b)). These modeling results taking into account the effect of recrystallization (Fig. 11(b)) are closer to the trend observed experimentally.

Our coupled model thus supports the hypothesis of a major influence of ferrite recrystallization state on austenite formation kinetics. This influence is modeled by introducing an effect of recrystallization on austenite nucleation sites, but it is very likely that recrystallization state also affects austenite formation by other means, including

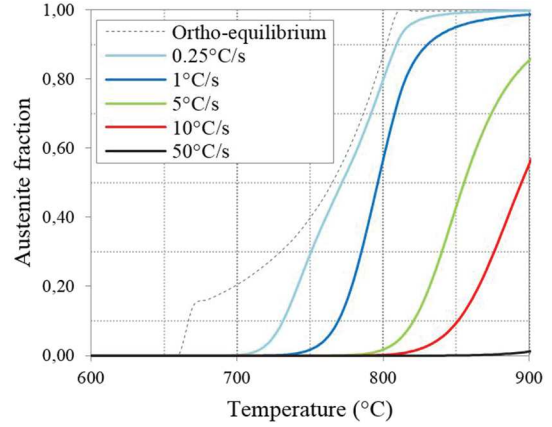


Fig. 10. Modeled austenite formation kinetics without the influence of ferrite recrystallization (constant number of nucleation sites: $N_\gamma = N_{\gamma 0}$).

cementite dissolution kinetics or carbon diffusion. The agreement with experimental points is not perfect due to this simplified approach on the one hand, but also due to natural dispersions in the sample [36], which are not taken into account in the model and to the use of adjustable parameters (see Table 1) that are not known with certainty.

In order to have a global picture of recrystallization and austenite formation kinetics depending on the heating rate, Fig. 12 represents the modeled phase fractions for the different investigated heating rates. Fig. 12 shows that recrystallization state when austenite forms is totally different depending on the heating rate. In particular, modeling results indicate that recrystallization is completed in case of heating at 0.25 °C/s (Fig. 12(a)) while it did not start in case of heating at 50 °C/s (Fig. 12(e)).

The modeled temperature ranges for which recrystallization and austenite formation occur during continuous heating at various heating rates are summarized in Fig. 13, representing the temperatures for which the modeled austenite fraction and fraction of recrystallized ferrite (defined as the ratio of recrystallized ferrite to total ferrite) are 0.10 and 0.90. Modeling results show that the temperature range of recrystallization is strongly shifted towards higher temperatures while the temperature range of austenite formation is only slightly affected by the increase of heating rate, due to the influence of recrystallization. The retardation of recrystallization combined with the acceleration of austenite formation due to the promoting effect of a less advanced recrystallization state lead to the overlap of the two mechanisms in case of high heating rates (Fig. 13).

Modeled austenite fraction obtained using the same parameters in case of 120 s soaking at 750 °C after heating at 1 °C/s or 10 °C/s is displayed in Fig. 14. Modeling the influence of recrystallization on austenite nucleation sites leads to higher austenite fraction from the first stages of soaking after fast heating, which is in agreement with experimental results. However, modeling results indicate that the austenite fractions become equal for the two heating rates after 80 s and do

Table 1

Values of the key parameters used in the model.

Parameter	Symbol	Unit	Values reported in the literature	Value used in the model
Dislocation density	ρ	m^{-2}	$1 \cdot 10^{14} < \rho < 1 \cdot 10^{15}$ [11,31]	
Grain boundary energy	γ_{bg}	$J \cdot m^{-2}$	$0.5 < \gamma_{bg} < 1$ [32,33]	1.0
Number density of recrystallization nucleation sites	N_{REX}	m^{-3}	$5 \cdot 10^{14} < N_{REX} < 1 \cdot 10^{16}$ [11,26,31]	$2 \cdot 10^{15}$
Pre-exponential factor for grain boundary mobility	D_{gb}^0	$m^2 \cdot s^{-1}$	$1 \cdot 10^{-2} < D_{gb}^0 < 1 \cdot 10^{-5}$ [31,33]	0.01
Activation energy for grain boundary mobility	Q_{gb}	$J \cdot mol^{-1}$	$140,000 < Q_{gb} < 230,000$ [26,31,34]	210,000
Minimum number density of austenite nucleation sites	$N_{\gamma 0}$	m^{-3}	$4 \cdot 10^{15} < N_{\gamma 0} < 1 \cdot 10^{16}$ [11,26]	$8 \cdot 10^{15}$
Activation energy for the interface mobility	Q_γ	$J \cdot mol^{-1}$	$Q_\gamma \sim 140,000$ [24,26]	140,000
Product of the pre-exponential factors for the mobility of the α/γ interface and the driving force for $\alpha \rightarrow \gamma$ transformation	$M_0 \Delta G_0$	$m \cdot s^{-1}$	$0.1 < M_0 \Delta G_0 < 300$ [26,35]	1

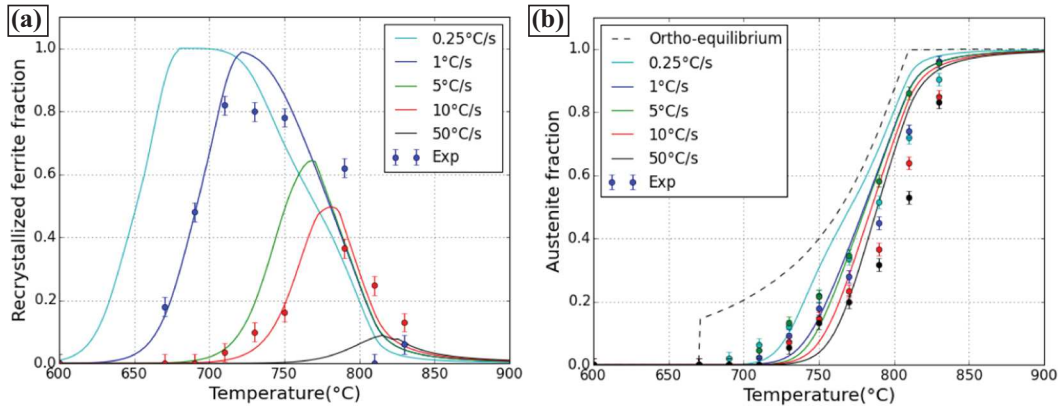


Fig. 11. Modeled results (a) recrystallized ferrite fraction (b) austenite fraction during continuous heating at different heating rates. Comparison with the experimental results

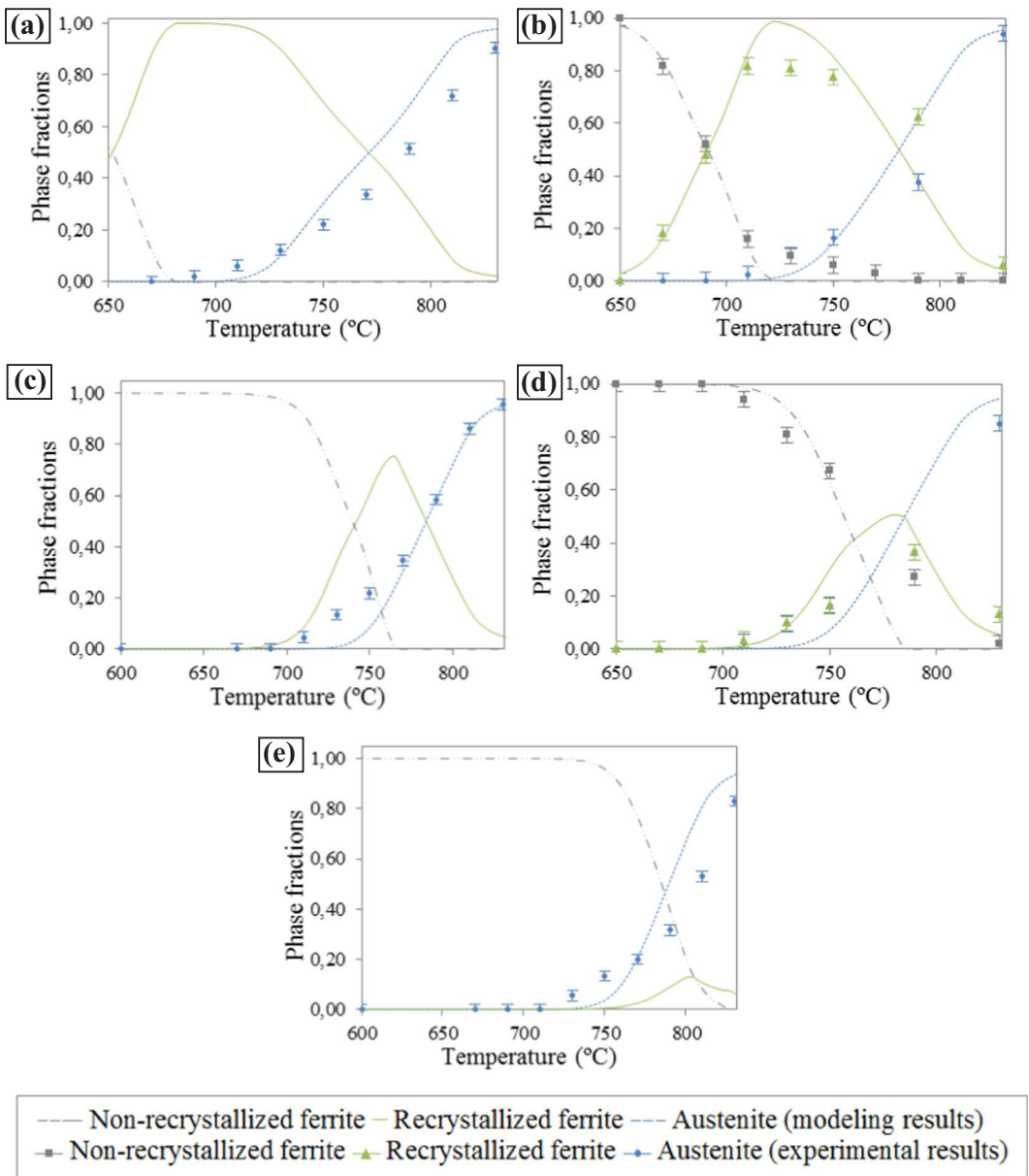


Fig. 12. Modeled phase fractions during continuous heating by taking into account the influence of recrystallisation on the density of austenite nucleation sites at (a) 0.25 °C/s (b) 1 °C/s (c) 5 °C/s (d) 10 °C/s and (e) 50 °C/s.

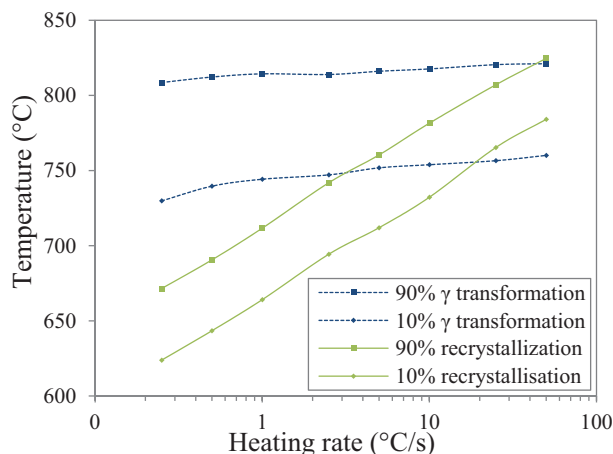


Fig. 13. Influence of heating rate on ferrite recrystallization and austenite formation temperature ranges during continuous heating: modeled temperatures corresponding to 10% and 90% transformation state taking into account the influence of recrystallization state on the density of austenite nucleation sites.

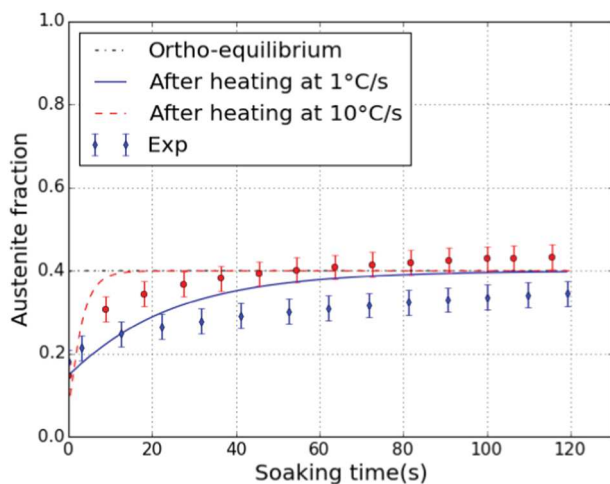


Fig. 14. Austenite fraction during 120 s soaking at 750 °C after heating at 1 °C/s or 10 °C/s. Modeling results in case where the density of austenite nucleation sites depends on recrystallization state as compared to experimental data.

not reproduce the experimental overshoot of the equilibrium fraction as the modeled austenite fraction is imposed to tend towards the equilibrium fraction at the soaking temperature via (Eq. 10).

5. Summary

In situ synchrotron X-ray diffraction experiments together with post-mortem metallographic analysis allowed the investigation of both ferrite recrystallization and austenite formation kinetics during annealing of ferrite-martensite cold-rolled microstructures depending on the process parameters of the annealing cycle. Experimental results revealed a strong shift in recrystallization to higher temperature when increasing the heating rate. Austenite formation kinetics has, however, limited sensitivity to the heating rate, indicating a promoting effect of high heating rates on austenite formation. Indeed, higher heating rates can lead to higher austenite fractions during continuous heating and systematically result in higher austenite fractions from the very beginning of isothermal soaking after heating. This unexpected trend is attributed to the promoting effect of a retarded recrystallization state on austenite formation in case of high heating rates. In particular, lower recrystallized fractions result in higher density of austenite nuclei. A

model coupling ferrite recrystallization and austenite formation during annealing of the bi-phased initial microstructure reproduces the trends observed experimentally, when the influence of recrystallization state on austenite formation is taken into account. If austenite fraction has limited sensitivity to the heating rate, the spatial distribution and size of austenite islands is, however, strongly modified by a change of heating rate. In particular, the overlap of ferrite recrystallization and austenite formation in case of high heating rates results in a higher density of austenite nuclei formed in prior martensite regions from the cold-rolled microstructure and leads to more heterogeneous microstructures.

Acknowledgements

This project was supported by the National Association of Research and Technology (ANRT – Project n°615/2014). The authors are grateful to DESY and Helmholtz-Zentrum Geesthacht for granting access to beamtime in P07B for the experiment I-20150130 EC.

Data availability

The raw/processed data required to reproduce these findings cannot be shared at this time due to technical or time limitations.

References

- [1] N. Pottore, N. Fonstein, I. Gupta, D. Bhattacharya, A family of 980MPa tensile strength advanced high strength steels with various mechanical property attributes, *Proc. Int. Conf. Adv. High Strength Sheet Steels Automot. Appl.* (2004) 119–130.
- [2] D.K. Matlock, G. Krauss, J.G. Speer, New microalloyed steel applications for the automotive sector, *Mater. Sci. Forum* 500–501 (2005) 87–96, <https://doi.org/10.4028/www.scientific.net/MSF.500-501.87>.
- [3] K. Bleck, W. Phiu-On, Effects of microalloying in multi phase steels for car body manufacture, *Texture Steels Other Mater*, 2009, pp. 145–163, https://doi.org/10.1007/978-1-84882-454-6_9.
- [4] D. Muljono, M. Ferry, D.P. Dunne, Influence of heating rate on anisothermal recrystallization in low and ultra-low carbon steels, *Mater. Sci. Eng. A* 303 (2001) 90–99, [https://doi.org/10.1016/S0921-5093\(00\)01882-7](https://doi.org/10.1016/S0921-5093(00)01882-7).
- [5] J. Huang, W.J. Poole, M. Militzer, Austenite formation during intercritical annealing, *Metall. Mater. Trans. A* 35 (2004) 3363–3375, <https://doi.org/10.1007/s11661-004-0173-x>.
- [6] C. Philippot, J. Drillet, P. Maugis, V. Hebert, M. Dumont, Austenite formation in a ferrite/martensite cold-rolled microstructure during annealing of advanced high-strength steels, *Metall. Res. Technol.* 111 (2014), <https://doi.org/10.1051/metal/2014004>.
- [7] A. Chbihi, D. Barbier, L. Germain, A. Hazotte, M. Gouné, Interactions between ferrite recrystallization and austenite formation in high-strength steels, *J. Mater. Sci.* 49 (2014) 3608–3621, <https://doi.org/10.1007/s10853-014-8029-2>.
- [8] H. Azizi-Alizami, M. Militzer, W.J. Poole, Austenite formation in plain low-carbon steels, *Metall. Mater. Trans. A Phys. Metall. Mater. Sci.* 42 (2011) 1544–1557, <https://doi.org/10.1007/s11661-010-0551-5>.
- [9] P. Li, J. Li, Q. Meng, W. Hu, D. Xu, Effect of heating rate on ferrite recrystallization and austenite formation of cold-roll dual phase steel, *J. Alloys Compd.* 578 (2013) 320–327, <https://doi.org/10.1016/j.jallcom.2013.05.226>.
- [10] G. Liu, J. Li, S. Zhang, J. Wang, Q. Meng, Dilatometric study on the recrystallization and austenization behavior of cold-rolled steel with different heating rates, *J. Alloys Compd.* 666 (2016) 309–316, <https://doi.org/10.1016/j.jallcom.2016.01.137>.
- [11] M. Kulakov, W.J. Poole, M. Militzer, The effect of the initial microstructure on recrystallization and austenite formation in a DP600 steel, *Metall. Mater. Trans. A* 44 (2013) 3564–3576.
- [12] R. Song, N. Fonstein, H. Jun, N. Pottore, D. Bhattacharya, S. Jansto, Effects of Nb on microstructural evolution and mechanical properties of low-carbon cold-rolled dual-phase steels, *Metallogr. Microstruct. Anal.* 3 (2014) 174–184.
- [13] C. Capdevila, T. De Cock, C. Garcia-Mateo, F. Caballero, Influence of second phase particles on recrystallisation of cold-rolled low carbon microalloyed steels during isothermal annealing, *Mater. Sci. Forum* 500–501 (2005) 803–810.
- [14] A. Staron, P. Fischer, T. Lippmann, T. Stark, A., Daneshpour, S., Schnubel, D., Uhlmann, E., Gerstenberger, R., Camin, B., Reimers, W., Eidenberger, E., Clemens, H., Huber, N. and Schreyer, In situ experiments with synchrotron high-energy X-rays and neutrons, *Adv. Eng. Mater.* 13 (2011) 658–663. <https://doi.org/10.1002/adem.201000297>.
- [15] A.P. Hammersley, FIT2D: an introduction and overview, *ESRF Intern. Rep. ESRF97HA02*, 1997, p. 58.
- [16] J. Rodríguez-Carvajal, Recent advances in magnetic structure determination by neutron powder diffraction, *Phys. B Phys. Condens. Matter.* 192 (1993) 55–69, [https://doi.org/10.1016/0921-4526\(93\)90108-1](https://doi.org/10.1016/0921-4526(93)90108-1).
- [17] E.M. Lauridsen, S. Schmidt, S.F. Nielsen, L. Margulies, H.F. Poulsen, D.J. Jensen, Non-destructive characterization of recrystallization kinetics using three-dimensional X-ray diffraction microscopy, *Scr. Mater.* 55 (2006) 51–56, <https://doi.org/>

- 10.1016/j.scriptamat.2006.02.028.
- [18] F.J. Humphreys, M. Hatherly, *Recrystallization and Related Annealing Phenomena*, Elsevier S, 1995.
- [19] J. Agren, Kinetics of carbide dissolution, *Scand. J. Metall.* 20 (1990) 2–8.
- [20] C. Philippot, K. Hoummada, M. Dumont, J. Drillet, V. Hebert, P. Maugis, Influence of a 2-D defect on the partitioning during the formation of a cementite particle in steels, *Comput. Mater. Sci.* 106 (2015), <https://doi.org/10.1016/j.commatsci.2015.04.020>.
- [21] R.W. Cahn, *Physical Metallurgy*, Phys. Metall. III (1996) 2399–2500, <https://doi.org/10.1016/B978-044489875-3/50033-8>.
- [22] M. Kulakov, W.J. Poole, M. Militzer, A microstructure evolution model for intercritical annealing of a low-carbon dual-phase steel, *ISIJ Int.* 54 (2014) 2627–2636, <https://doi.org/10.2355/isijinternational.54.2627>.
- [23] M. Ollat, V. Massardier, D. Fabregue, E. Buscarlet, F. Keovilay, M. Perez, Modeling of the recrystallization and austenite formation overlapping in cold-rolled dual-phase steels during intercritical treatments, *Metall. Mater. Trans. A.* 48 (2017) 4486–4499, <https://doi.org/10.1007/s11661-017-4231-6>.
- [24] B. Zhu, M. Militzer, Phase-field modeling for intercritical annealing of a dual-phase steel, *Metall. Mater. Trans. A Phys. Metall. Mater. Sci.* 46 (2015) 1073–1084, <https://doi.org/10.1007/s11661-014-2698-y>.
- [25] C. Zheng, D. Raabe, Interaction between recrystallization and phase transformation during intercritical annealing in a cold-rolled dual-phase steel: a cellular automaton model, *Acta Mater.* 61 (2013) 5504–5517, <https://doi.org/10.1016/j.actamat.2013.05.040>.
- [26] C. Bos, M.G. Mecozzi, J. Sietsma, A microstructure model for recrystallisation and phase transformation during the dual-phase steel annealing cycle, *Comput. Mater. Sci.* 48 (2010) 692–699, <https://doi.org/10.1016/j.commatsci.2010.03.010>.
- [27] A.N. Kolmogorov, Statistical theory of crystallization of metals, *Bull. Russ. Acad. Sci.* 1 (1937) 355–359.
- [28] W.A. Johnson, R.F. Mehl, Reaction kinetics in processes of nucleation and growth, *Trans. Am. Inst. Min. Met. Eng.* 135 (1939) 416–458.
- [29] M. Avrami, Kinetics of phase change. III: granulation, phase change and microstructure, *J. Chem. Phys.* 9 (1941) 177–184.
- [30] S.J. Jones, H.K.D.H. Bhadeshia, Kinetics of the simultaneous decomposition of austenite into several transformation products, *Acta Mater.* 45 (1997) 2911–2920, [https://doi.org/10.1016/S1359-6454\(96\)00392-8](https://doi.org/10.1016/S1359-6454(96)00392-8).
- [31] C.W. Sinclair, C.R. Hutchinson, Y. Bréchet, The effect of Nb on the recrystallization and grain growth of ultra-high-purity α -Fe: a combinatorial approach, *Metall. Mater. Trans. A Phys. Metall. Mater. Sci.* 38 (2007) 821–830, <https://doi.org/10.1007/s11661-007-9106-9>.
- [32] C. Hutchinson, H. Zurob, C. Sinclair, Y. Brechet, The comparative effectiveness of Nb solute and NbC precipitates at impeding grain-boundary motion in Nb steels, *Scr. Mater.* 59 (2008) 635–637, <https://doi.org/10.1016/j.scriptamat.2008.05.036>.
- [33] H.S. Zurob, C.R. Hutchinson, Y. Brechet, G. Purdy, Modeling recrystallization of microalloyed austenite: effect of coupling recovery, precipitation and recrystallization, *Acta Mater.* 50 (2002) 3077–3094, [https://doi.org/10.1016/S1359-6454\(02\)00097-6](https://doi.org/10.1016/S1359-6454(02)00097-6).
- [34] D.Z. Yang, E.L. Brown, D.K. Matlock, G. Krauss, Ferrite recrystallization and austenite formation in cold-rolled intercritically annealed steel, *Metall. Trans. A.* 16 (1985) 1385–1392, <https://doi.org/10.1007/BF02658671>.
- [35] M. Gouné, J. Drillet, P. Maugis, Modelling of the interaction between phase transformation and precipitation: coupled kinetics in microalloyed multiphase steels, *Comput. Mater. Sci.* 55 (2012) 127–135, <https://doi.org/10.1016/j.commatsci.2011.11.027>.
- [36] M. Gouné, P. Maugis, The role of dispersions in modeling the kinetics of phase transformations, *Solid State Phenom.* 172 (2011) 279–284.